

Instability of neutron star matter in high magnetic field: constraint on central magnetic field of magnetars

Monika Sinha, Banibrata Mukhopadhyay

Department of Physics, Indian Institute of Science, Bangalore 560012, India

Abstract

Pulsars are believed to be magnetized neutron stars. Their surface magnetic field ranges from 10^8 to 10^{12} G. On the other hand, the magnetars have surface magnetic field $10^{14} - 10^{15}$ G. It is believed that at the center, the magnetic field may be higher than that at the surface. We study the effect of the magnetic field on the neutron star matter and hence on the mass-radius relation of neutron stars. We model the nuclear matter with the relativistic mean field approach considering the possibility of appearance of hyperons at higher density. We find that the effect of magnetic field on the matter of neutron stars and hence on the mass-radius relation is important when central magnetic field $\geq 10^{17}$ G. Moreover, if the central field is of the order of 10^{19} G, then the matter becomes unstable which limits the maximum magnetic field at the center of magnetars.

Keywords: magnetar/neutron star, equation of state of neutron star matter, hyperon matter, nuclear physics aspects of neutron stars

PACS: 26.60.-c, 26.60.Dd, 26.60.Kp, 97.10.Ld, 97.60.Jd

1. Introduction

Soon after the discovery of radio pulsar [1], the theoretical proposition of neutron star (NS) [2] drew much attention. At the core of a NS, the matter, composed of neutrons, protons, electrons, and sometimes muons, is highly degenerate with density in the range of $10^{14} - 10^{15}$ gm/cc. Naturally, the constituent particles therein interact via nuclear forces, forming a non-ideal

Email addresses: msinha@physics.iisc.ernet.in (Monika Sinha),
bm@physics.iisc.ernet.in (Banibrata Mukhopadhyay)

nuclear fluid. However, the nature of nuclear forces at this high density and the internal composition, especially the composition of matter in the inner most core of the NS, are not well understood yet. There are many theoretical models of nuclear matter at high density describing different equations of state for the matter. Based on different equations of state, different mass-radius relations of NS are obtained. Consequently, only way to constrain the equations of state is comparing the theoretical results with observed properties of NS.

With the detection of pulsars, it was also observed that the pulse period slowly increases in a very regular manner. Consequently, pulsars were successfully modeled as magnetized rotating NSs [3, 4, 5]. This model successfully describes the spin-down power of the Crab pulsar and other pulsars. This description requires a surface magnetic field $10^{11} - 10^{13}$ G for the pulsars detected at the beginning. Later on, more observations broadened this range of the magnetic field with the discovery of millisecond pulsars [6]. This class of pulsars has a much lower surface magnetic field of $10^8 - 10^{10}$ G [7]. In the recent past pulsars with a very high rate of change of period (period derivatives) have been observed [8, 9], implying a high surface field up to 10^{14} G. Another class of pulsars has been observed which is the accreting X-ray pulsar [10]. For this class, the surface magnetic field varies from 10^8 to 10^{13} G.

Anomalous X-ray pulsars (AXPs) were discovered in early 80s, which show periods in a relatively narrow range of $5 - 11$ s and have large period derivatives [11]. In early days, they were believed to be unusual accreting NSs, whereas, later surveys detected no companions for these candidates. The large value of period derivatives implies a surface magnetic field as high as $10^{14} - 10^{15}$ G. This helps in explaining the X-ray luminosities, powered by magnetic field decay, without any accretion. However, until the discovery of soft γ -ray repeaters (SGRs), such high values of surface magnetic field were not acceptable. SGRs show brief intense bursts of soft γ -rays. From the peak luminosities of the bursts, SGRs are identified as NSs with very strong surface magnetic field ($\sim 10^{14} - 10^{15}$ G) [12, 13]. Now both AXP and SGR are believed to be strongly magnetized NSs with different variations, which are popularly known as magnetars [11, 14, 15, 16].

The existence of a magnetar motivates to study the effects of strong magnetic field on NS properties. A strong magnetic field affects, the structure of a NS through its influence on the underlying metric [17, 18] and equation of state (EoS) through the Landau quantization of charged particles and

then the interaction of magnetic moments of charged particles (and even the anomalous magnetic moment (AMM) of neutral particles) with the magnetic field. In the present paper, we plan to study the effect of magnetic field on the EoS of highly dense matter. Generally, the effect of magnetic field on the EoS of matter is significant when the magnetic field $\mathcal{B} > 10^{18}$ G. For the nuclear matter with a n - p - e system, the effect of magnetic field was studied by several authors [19, 20, 21, 22, 23]. However, the composition of the core of a NS is very uncertain as the density reaches 10–15 times the normal matter density. At this high density, the quarks may be deconfined, making quark matter, or the hyperons may appear, making hyperonic matter. Another hypothesis is that the whole star is made of deconfined quark matter, which is known as strange star (SS). The effect of magnetic field on quark matter using the MIT bag model has been studied in different literature [24, 25, 26]. There are other models of quark matter with phenomenological density dependent quark masses [27, 28, 29, 30]. Broderick et al. [31] studied the effect of strong magnetic field on hyperonic matter. In their study, the field strength does not depend on density. However, in realistic situation, it is believed that the field strength is higher at core than that at surface of a NS. Therefore, with radius, and hence with density, the field strength should vary. In the present work, we plan to study the influence of the strong magnetic field on the hyperonic matter and hence on the mass-radius relation of NSs with hyperonic matter in the core with a density dependent magnetic field.

The paper is organized as follows. In the next section we describe the model of hadronic matter at high densities in the presence of magnetic field. Subsequently, we discuss the numerical results in section 3. Finally, we summarize the results in the last section.

2. Model

Among many theoretical models of dense nuclear matter, the relativistic mean field theory of nuclear matter, also known as Walecka model [32], successfully describes the nuclear ground state properties and elastic scattering [32, 33, 34, 35]. In this model, the nucleons in matter interact among each other through three meson fields: the isoscalar-scalar meson σ , isoscalar-vector meson ω , and isovector-vector meson ρ . However, the original Walecka model [32] predicts very high incompressibility of nuclear matter. One of the ways to solve this problem is by introducing cubic and quartic self interaction terms for the scalar field into the Lagrangian [36]. With this prescription,

the EoS of nuclear matter and the properties of NSs were studied extensively [37, 38, 39, 40, 41].

In the present paper, we employ this idea to construct the model of dense matter. In addition, we consider the possibility of appearance of hyperons ($\Lambda, \Sigma^-, \Sigma^0, \Sigma^+, \Xi^-, \Xi^0$) and muons (μ^-) at higher density. The Lagrangian density of matter under consideration is then given by [37]

$$\begin{aligned} \mathcal{L}_B = & \sum_B \bar{\psi}_B (i\gamma_\mu D^\mu - m_B + g_{\sigma B}\sigma - g_{\omega B}\gamma_\mu\omega^\mu - g_{\rho B}\gamma_\mu\boldsymbol{\tau}_B \cdot \boldsymbol{\rho}^\mu) \psi_B \\ & + \frac{1}{2}\partial_\mu\sigma\partial^\mu\sigma - \frac{1}{2}m_\sigma^2\sigma^2 - U(\sigma) \\ & - \frac{1}{4}\omega_{\mu\nu}\omega^{\mu\nu} + \frac{1}{2}m_\omega^2\omega_\mu\omega^\mu - \frac{1}{4}\boldsymbol{\rho}_{\mu\nu} \cdot \boldsymbol{\rho}^{\mu\nu} + \frac{1}{2}m_\rho^2\boldsymbol{\rho}_\mu \cdot \boldsymbol{\rho}^\mu \\ & + \sum_{l=e,\mu} \bar{\psi}_l (i\gamma_\mu D^\mu - m_l) \psi_l - \frac{1}{4}F_{\mu\nu}F^{\mu\nu}. \end{aligned} \quad (1)$$

Here, B indicates all baryons present in the matter. The scalar self interaction term [36, 37] is

$$U(\sigma) = \frac{1}{3} g_1 m_N (g_{\sigma N}\sigma)^3 + \frac{1}{4} g_2 (g_{\sigma N}\sigma)^4, \quad (2)$$

and

$$\omega_{\mu\nu} = \partial_\nu\omega_\mu - \partial_\mu\omega_\nu, \quad (3)$$

$$\boldsymbol{\rho}_{\mu\nu} = \partial_\nu\boldsymbol{\rho}_\mu - \partial_\mu\boldsymbol{\rho}_\nu, \quad (4)$$

$$D^\mu = \partial^\mu + ieQA^\mu, \quad (5)$$

with the choice of gauge $A^\mu \equiv (0, -y\mathcal{B}, 0, 0)$, where \mathcal{B} being the magnitude of magnetic field and eQ the charge of the particle, e the positive unit of charge. For this particular gauge choice $\vec{\mathcal{B}} = \mathcal{B}\hat{z}$. This does not mean any preferred choice of direction, but only specifies the coordinate axes. $\psi_B, \psi_l, \sigma, \omega$ and $\boldsymbol{\rho}$ are fields of baryons, leptons, σ -mesons, ω -mesons and ρ -mesons, with masses $m_B, m_l, m_\sigma, m_\omega$ and m_ρ respectively, $g_{\sigma B}, g_{\omega B}$ and $g_{\rho B}$ are coupling constants for interactions of σ, ω and ρ mesons respectively with the baryon B . In the mean field approximation approach, the baryons acquire the effective masses as

$$m_B^* = m_B - g_{\sigma B}\sigma, \quad (6)$$

where σ is given by its ground state expectation value

$$\langle \sigma \rangle = \sigma = \frac{1}{m_\sigma^2} \left(\sum_B g_{\sigma B} n_S^{(B)} - \frac{\partial U}{\partial \sigma} \right), \quad (7)$$

with the scalar density

$$n_S^{(B)} = \frac{2}{(2\pi)^3} \int_0^{p_F^{(B)}} \frac{m_B^*}{\sqrt{p_B^2 + m_B^{*2}}} d^3 p_B, \quad (8)$$

where p_B is the momentum and $p_F^{(B)}$ the Fermi momentum of the baryon B .

In the presence of magnetic field, the motion of the charged particles is Landau quantized in the perpendicular direction to the magnetic field. With the given gauge choice for $\vec{\mathcal{B}}$ described above, the positive energy solution for any charged particle is given by

$$\psi = e^{-i(E_n t - p_x x - p_z z)} U_s(y, n, \mathbf{p}), \quad (9)$$

where p_x , p_z are the components of momentum along x and z directions respectively, E_n the energy at the n th Landau level and U_s the suitable spinor. For positively charged baryons, up and down spinors are given by

$$U_\uparrow(y_B, n, \mathbf{p}_B) = \sqrt{E_n^{(B)} + m_B^*} \begin{bmatrix} I_n(\xi_B) \\ 0 \\ \frac{p_z^{(B)}}{E_n^{(B)} + m_B^*} I_n(\xi_B) \\ \frac{\sqrt{2ne\mathcal{B}}}{E_n^{(B)} + m_B^*} I_{n-1}(\xi_B) \end{bmatrix}, \quad (10)$$

$$U_\downarrow(y_B, n, \mathbf{p}_B) = \sqrt{E_n^{(B)} + m_B^*} \begin{bmatrix} 0 \\ I_{n-1}(\xi_B) \\ \frac{\sqrt{2ne\mathcal{B}}}{E_n^{(B)} + m_B^*} I_n(\xi_B) \\ \frac{-p_z^{(B)}}{E_n^{(B)} + m_B^*} I_{n-1}(\xi_B) \end{bmatrix} \quad (11)$$

and for negatively charged baryons,

$$U_{\uparrow}(y_B, n, \mathbf{p}_B) = \sqrt{E_n^{(B)} + m_B^*} \begin{bmatrix} I_{n-1}(\xi_B) \\ 0 \\ \frac{p_z^{(B)}}{E_n^{(B)} + m_B^*} I_{n-1}(\xi_B) \\ \frac{-\sqrt{2ne\mathcal{B}}}{E_n^{(B)} + m_B^*} I_n(\xi_B) \end{bmatrix}, \quad (12)$$

$$U_{\downarrow}(y_B, n, \mathbf{p}_B) = \sqrt{E_n^{(B)} + m_B^*} \begin{bmatrix} 0 \\ I_n(\xi_B) \\ \frac{-\sqrt{2ne\mathcal{B}}}{E_n^{(B)} + m_B^*} I_{n-1}(\xi_B) \\ \frac{-p_z^{(B)}}{E_n^{(B)} + m_B^*} I_n(\xi_B) \end{bmatrix}. \quad (13)$$

The spinors of negatively charged leptons are same as that of negatively charged baryons except m_B^* replaced by m_l which is the mass of the leptons. Here

$$I_n(\xi) = \left(\frac{\sqrt{e|Q|\mathcal{B}}}{n!2^n\sqrt{\pi}} \right)^{1/2} e^{-\xi^2/2} H_n(\xi) \quad (14)$$

and

$$\xi = \sqrt{e|Q|\mathcal{B}} \left(y + \frac{p_x}{eQ\mathcal{B}} \right), \quad (15)$$

with $H_n(\xi)$ being the Hermite polynomial. The momentum in the x - y plane is quantized and hence the energy in the n th Landau level is given by

$$E_n = \sqrt{p_z^2 + m^2 + 2ne|Q|\mathcal{B}}. \quad (16)$$

For positively charged particles, e.g. proton, $n = 0, 1, 2, \dots$ for the spin up states and $n = 1, 2, 3, \dots$ for the spin down states. However, for negatively charged particles, e.g. electron, $n = 0, 1, 2, \dots$ for the spin down states and $n = 1, 2, 3, \dots$ for the spin up states. The number density of neutral baryons is given by

$$n_N^{(B)} = \frac{1}{3\pi^2} p_F^{(B)3}, \quad (17)$$

and the number densities of charged baryons and leptons are given by

$$n_C^{(B),(l)} = \frac{e|Q|\mathcal{B}}{2\pi^2} \sum_{n=0}^{n_{max}} (2 - \delta_{n,0}) \sqrt{p_F^{(B,l)^2} - 2ne|Q|\mathcal{B}}, \quad (18)$$

where n_{max} is given by

$$n_{max} = \text{Int} \left(\frac{p_F^2}{2e|Q|\mathcal{B}} \right). \quad (19)$$

The scalar density of neutral baryons is

$$n_{S,N}^{(B)} = \frac{m_B^{*3}}{\pi^2} \left(\frac{p_F^B \mu_B^*}{2m_B^{*2}} - \frac{1}{2} \ln \frac{p_F^B + \mu_B^*}{m_B^*} \right), \quad (20)$$

while for charged baryons it is

$$n_{S,C}^{(B)} = \frac{e|Q|\mathcal{B}}{2\pi^2} m_B^* \sum_{n=0}^{n_{max}} (2 - \delta_{n,0}) \ln \frac{p_B(n) + \mu_B^*}{\sqrt{m_B^{*2} + 2ne|Q|\mathcal{B}}}, \quad (21)$$

with

$$\mu_B^* = \sqrt{p_F^{(B)^2} + m_B^{*2}} \text{ and } p_B(n) = \sqrt{p_F^{(B)^2} - 2ne|Q|\mathcal{B}}. \quad (22)$$

The chemical potential of baryons is $\mu_B = \mu_B^* + \omega^0 g_{\omega B} + \rho_3^0 I_3^{(B)} g_{\rho B}$ where

$$\omega^0 = \frac{1}{m_\omega^2} \sum_B g_{\omega B} n_B \text{ and } \rho_3^0 = \frac{1}{m_\rho^2} \sum_B g_{\rho B} I_3^{(B)} n_B \quad (23)$$

which are the ground state expectation values of ω and ρ_3 fields, and $I_3^{(B)}$ is the isospin projection of the baryon B . The total baryonic number density of the matter is $n_b = \sum_B n_B$. The matter is neutral in charge, which implies $n_p + n_{\Sigma^+} = n_{\Xi^-} + n_{\Sigma^-} + n_e + n_\mu$. In addition, the matter is in beta-equilibrium, which gives the condition $\mu_n = \mu_p + \mu_e$.

The total energy density of matter is then

$$\begin{aligned} \varepsilon = & \frac{1}{2} m_\sigma^2 \sigma^2 + U(\sigma) + \frac{1}{2} m_\omega^2 \omega^2 + \frac{1}{2} m_\rho^2 \rho_3^2 \\ & + \sum_N \frac{1}{8\pi^2} \left(2p_F^{(N)} \mu_N^{*3} - p_F^{(N)} m_N^{*2} \mu_N^* - m_N^{*4} \ln \left[\frac{p_F^{(N)} + \mu_N^*}{m_N^*} \right] \right) \end{aligned}$$

$$\begin{aligned}
& + \frac{e|Q|\mathcal{B}}{(2\pi)^2} \sum_C \sum_{n=0}^{n_{max}} (2 - \delta_{n,0}) \\
& \times \left(p_C(n) \mu_C^* + (m_C^{*2} + 2ne|Q|\mathcal{B}) \ln \left[\frac{p_C(n) + \mu_C^*}{\sqrt{(m_C^{*2} + 2ne|Q|\mathcal{B})}} \right] \right) \\
& + \frac{e|Q|\mathcal{B}}{(2\pi)^2} \sum_{l=e,\mu} \sum_{n=0}^{n_{max}} (2 - \delta_{n,0}) \\
& \times \left(p_l(n) \mu_l + (m_l^2 + 2ne|Q|\mathcal{B}) \ln \left[\frac{p_l(n) + \mu_l}{\sqrt{(m_l^2 + 2ne|Q|\mathcal{B})}} \right] \right) \\
& + \frac{\mathcal{B}^2}{8\pi}, \tag{24}
\end{aligned}$$

where N is charge neutral baryons, C charged baryons and $p_l(n) = \sqrt{p_F^{(l)2} - 2ne|Q|\mathcal{B}}$. The total pressure is then

$$P = \sum_B \mu_B n_B + \sum_l \mu_l n_l - \varepsilon. \tag{25}$$

The relation between energy density and pressure describes the EoS of the matter.

Now we employ this EoS to get the mass-radius relation of a NS with hyperon in its core. We consider the stationary and axisymmetric metric, which can be written as [42]

$$ds^2 = e^{\gamma+\nu} dt^2 + e^{2\alpha} (dr^2 + r^2 d\theta^2) + e^{\gamma-\nu} r^2 \sin^2 \theta (d\phi - \varpi dt)^2, \tag{26}$$

where ν, γ, α and ϖ are functions of r and θ only. Next, we construct and solve the equations of hydrostatic equilibrium following the previous authors [42].

3. Results and discussion

Nucleon-meson coupling constants are chosen in such a way that the nuclear matter properties can be reproduced as the binding energy $E/B = -16.3$ MeV, the saturation density $n_0 = 0.153 \text{ fm}^{-3}$, the asymmetry energy coefficient $a_{asy} = 32.5$ MeV and the incompressibility $K = 240$ MeV, and are taken from previous work [37]. The hyperon- ω coupling constants are

determined from SU(6) symmetry of the quark model [43, 44, 45]. The hyperon- σ coupling constants, however, are determined from the potential depth of hyperons in normal nuclear matter given by

$$U_Y = -g_{\sigma Y}\sigma + g_{\omega Y}\omega_0, \quad (27)$$

where Y corresponds to hyperon. We take the potential depth for Λ -hyperon $U_\Lambda = -30 \text{ MeV}$, as obtained from the analysis of Λ -hypernuclei [43, 46]. From various experimental data [46, 47] for Ξ -hypernuclei, we obtain the potential depth for Ξ -hyperon $U_\Xi = -18 \text{ MeV}$. Recent Σ -hypernuclei data indicate that the corresponding potential depth to be repulsive [48] and we take $U_\Sigma = 30 \text{ MeV}$. Note importantly that earlier work [31] assumed hyperon-meson coupling constants to be fixed fractions of respective nucleon-meson coupling constants and for all the hyperons these fractions are same for a given meson. Hence, unlike our model, in that work the first appeared hyperon is Σ^+ , which does not appear at all (see Table 1) in our model.

In a realistic situation, the magnetic field at the core may be higher than that at the surface and gradually may decrease towards the surface. For the magnetars, the maximum surface magnetic field is 10^{15} G . For this case, the core magnetic field may be of the order of $10^{17} - 10^{18} \text{ G}$. Without any proper knowledge of magnetic field configuration inside a NS, following previous work [49] here we adopt a magnetic field profile

$$\mathcal{B}(n_b/n_0) = \mathcal{B}_s + \mathcal{B}_c \left\{ 1 - e^{-\beta \left(\frac{n_b}{n_0}\right)^\gamma} \right\}, \quad (28)$$

where β and γ are two parameters determining the magnetic field profile with given \mathcal{B}_s and \mathcal{B}_c , and n_b is the total baryon number density. We consider different values of field at the center, whereas surface field strength is taken to be $\mathcal{B}_s = 10^{15} \text{ G}$. We notice that the different values of \mathcal{B}_s do not affect the EoS considerably, and thus we do not show the results with other \mathcal{B}_s . In the above parametrization, the magnetic field strength depends on the baryon number density. However, at each density the field is uniform and constant.

3.1. Equation of states

We compute the EoS self-consistently with the condition of beta-equilibrium and charge neutrality. It is found that, as described by the Figures given below, the effect of magnetic field is important for $\mathcal{B}_c \geq 10^{17} \text{ G}$. However, for $\mathcal{B}_c < 10^{18} \text{ G}$, the effect is significant only when the field reaches \mathcal{B}_c at a very

Threshold densities	
μ^-	0.9
Λ	2.6
Ξ^-	3.1
Ξ^0	5.7

Table 1: Threshold densities for muons and hyperons to appear in units of n_0 .

low density, away from the center, and remains almost constant up to center. Therefore, we restrict our study with $\mathcal{B}_c \sim 10^{18}$ G. At lower densities, the matter is composed of only neutrons, protons and electrons. Hence, at the low density regime, the particles which are affected by the magnetic field are electrons and protons. Since the electrons are highly relativistic, electron Fermi momentum is very large compared to electron mass. Therefore, the number of occupied Landau levels by electrons is very large, even though the field strength under consideration is larger than the critical field strength of electron by several orders. On the other hand, the field strength under consideration is very less than the critical field strength of protons. Consequently, the number of occupied Landau levels by protons is also large. As density increases, the heavier particles appear gradually. In addition, the magnetic field increases with the increase of density. As a result, the number of occupied Landau levels gradually decreases for every species. The threshold densities for muons and other hyperons to appear for $\mathcal{B}_c = 10^{18}$ G are given in Table 1. The threshold densities for various species to appear do not differ from their respective values when the magnetic field is absent.

In Fig. 1 we show the EoSs with and without magnetic field when the magnetic field profile corresponds to $\beta = 0.1$ and $\gamma = 1$ [see Eq. (28)]. We observe that the EoS becomes softer with the increase of \mathcal{B}_c . Here we should mention that, when the field strength is high enough, the field energy and the field pressure are not negligible. In calculating the EoS, we thus add this contribution too which is necessary to construct the structure of NSs.

3.2. Mass-radius relations

With the above EoSs, the structure of NSs with and without rotation is constructed. In this preliminary study of NS structure, we do not include anisotropic solutions based on the general relativity which is important in

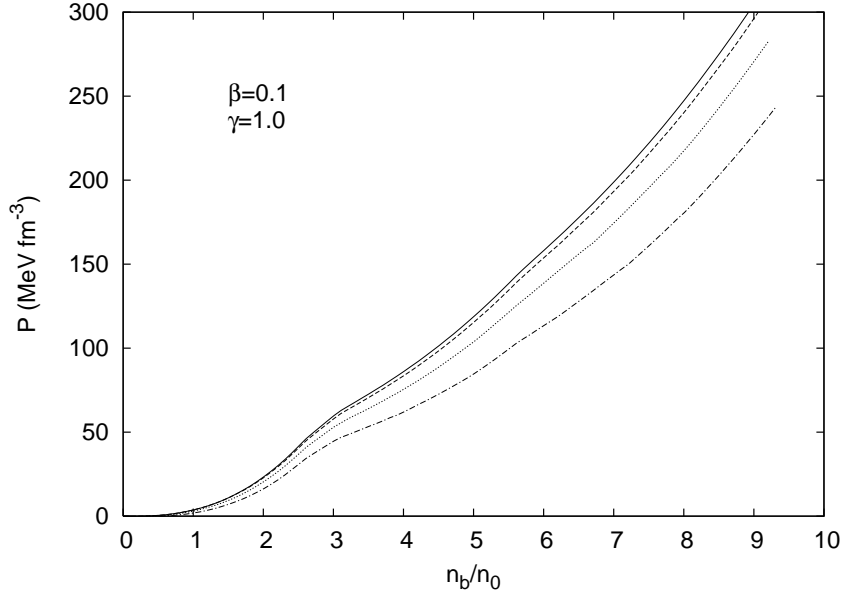


Figure 1: Variation of P as a function of normalized baryon number density. The solid curve is for without magnetic field. The dashed, dotted and dot-dashed curves correspond to $\mathcal{B}_c = 10^{18}$, 2×10^{18} and 3×10^{18} G respectively.

strong magnetic field. Without any rotation, the Einstein's equation leads to the Tolman-Oppenheimer-Volkoff (TOV) equation

$$\frac{dP}{dr} = -\frac{[\varepsilon(r) + P(r)][M(r) + 4\pi r^3 P(r)]}{r[r - 2M(r)]}, \quad (29)$$

where r is the distance from the center of the star and $M(r)$ the mass enclosed within r . The radius of a star (R) is the distance from the center at which the pressure becomes zero. For different central densities, stars with different masses and radii are formed. In Fig. 2 the mass-radius relations for static stars which correspond to EoSs described in Fig. 1 are shown. Since the effect of magnetic field softens the EoS, in the presence of magnetic field the maximum mass is less than that for without magnetic field. Stars with rotation, as expected, have larger radii than their static counterpart. In Figs. 3 and 4 we show the corresponding mass-radius relations for rotating NSs. In both the cases, the maximum masses in presence of the magnetic field are less than that in absence of the magnetic field.

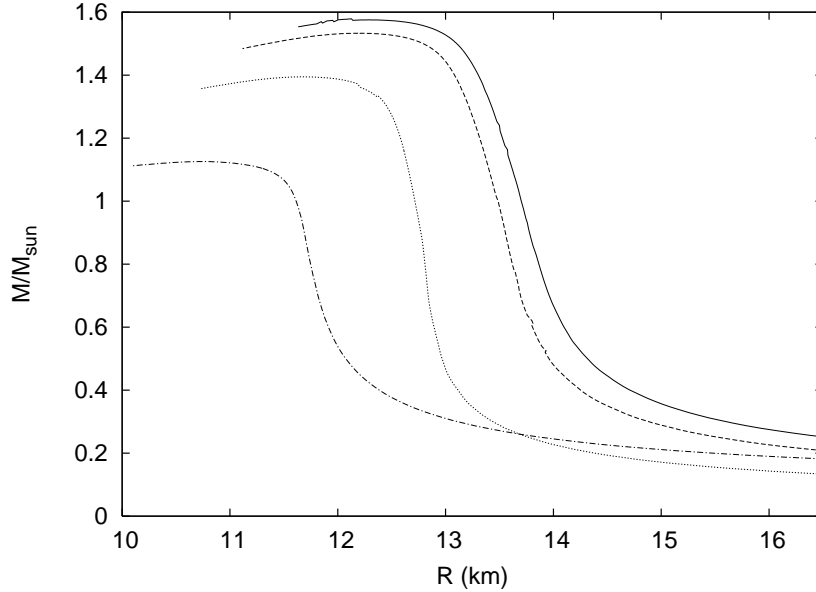


Figure 2: Mass-radius relations without rotation. The solid curve is for without magnetic field. The dashed, dotted and dot-dashed curves correspond to $\mathcal{B}_c = 10^{18}$, 2×10^{18} and 3×10^{18} G respectively.

3.3. Matter instability due to magnetic field

It has been noted that there is an onset of matter instability for certain sets of β and γ (which correspond to different magnetic field profiles) for every \mathcal{B}_c . Now we explore EoSs for different magnetic field profiles to understand the instability. Figures 5a and 6a show the variations of P at $\mathcal{B}_c = 10^{18}$ and 3×10^{18} G respectively, for different sets of β and γ . For each β , we take minimum γ to be 1 for which \mathcal{B} varies very slowly with n_b (see Figs. 5b and 6b). The maximum value of γ for every β has been chosen in such a way that beyond a certain value of n_b , P ceases to increase (and decreases) with the further increase of n_b . This implies that the matter becomes unstable after that value of n_b . Keeping β constant if γ decreases, then instability disappears at some value of γ and the EoS tends to become that for without magnetic field. The point to note is that if β decreases, the instability occurs at larger values of γ and n_b , which is evident from Figs. 5a and 6a.

The instability occurs because the magnetic pressure contributes negatively to the matter pressure as reflected from the Eqs. (24) and (25). Since the field strength increases with the increase of density, more negative contri-

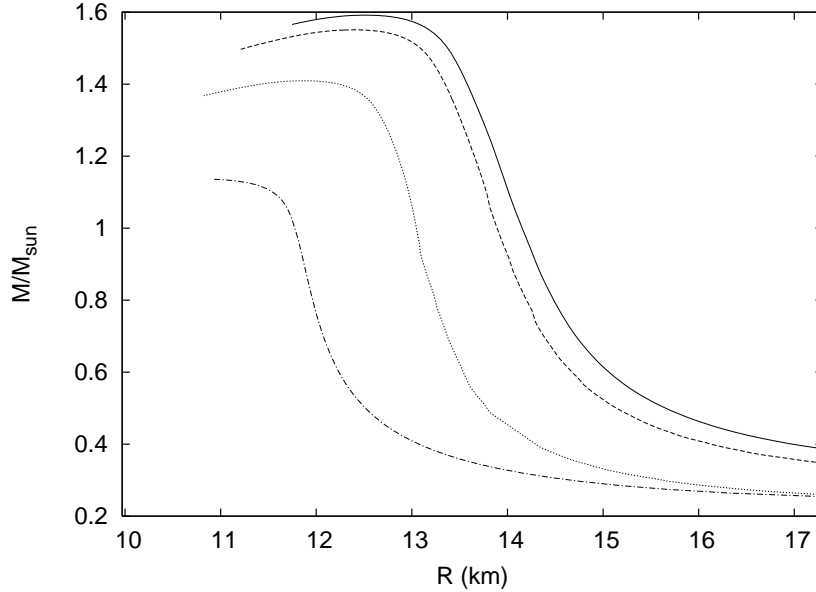


Figure 3: Same as Fig. 2, except for rotating NSs with rotational frequency $\Omega = 2000 \text{ s}^{-1}$.

bution is added to the pressure, and finally, at a certain density, the pressure ceases to increase with the increase of the density. This effect has not been discussed in any earlier literature to the best of our knowledge. This is consistent with the result of softening the EoS with the increase of magnetic field. Since the softening of the EoS implies that with the energy density the rate of increase of pressure decreases, above a certain value of magnetic field, the rate becomes zero, and subsequently becomes negative. That is why, above a certain value of magnetic field the matter becomes unstable. This constrains the value of central magnetic field of a NS having high surface magnetic field, e.g. magnetar. In this context, it is worth mentioning that the inclusion of AMM effect [31] stiffens the EoS, which dominates over the effect due to Landau quantization on EoS when field strength is $> 5 \times 10^{18} \text{ G}$. This stiffening is only possible when the field pressure is not considered in obtaining the EoS. However, the inclusion of field pressure further softens the EoS, as discussed above.

When the field strength is $\sim 5 \times 10^{19} \text{ G}$, the deviation in EoSs between the cases with and without AMM effect is significant throughout the density range [31]. However, this deviation is much small compared to that due to the extra effect arised from field pressure. Hence, at such a strong magnetic

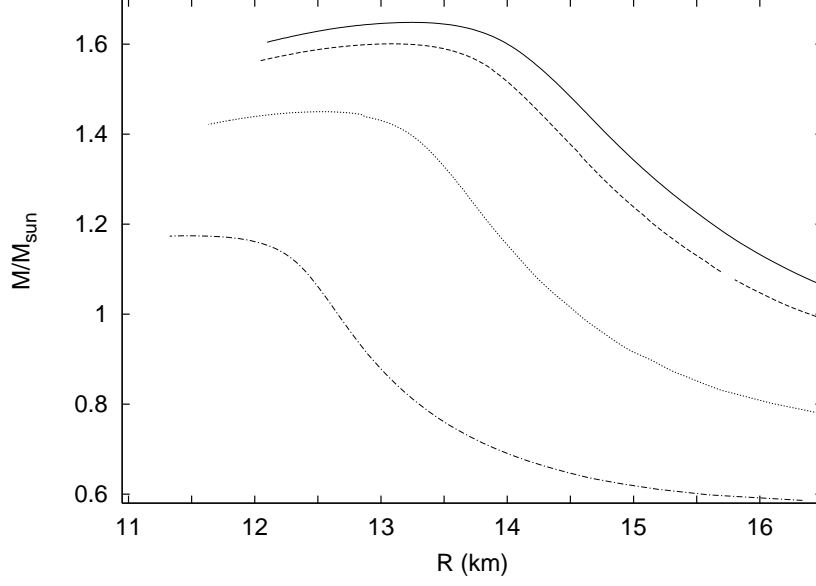


Figure 4: Same as Fig. 2, except for rotating NSs with rotational frequency $\Omega = 4000 \text{ s}^{-1}$.

field, AMM effect is unable to stiffen the EoS. It is, however, seen that when the field strength is near $5 \times 10^{18} \text{ G}$, AMM effect is insignificant at high density, but significant at low density. However, one should also remember that this result is obtained by considering constant field strength over the whole range of density. Thus, in the realistic case, when the field strength is several orders lower than 10^{18} G at low density, i.e., near the surface, AMM effect does not play any role in modifying the EoS. Therefore, we do not consider the AMM effect in our calculation while $\mathcal{B}_c \leq 10^{19} \text{ G}$.

In Fig. 7, the mass-radius relations for different \mathcal{B}_c as well as that without magnetic field have been shown. We notice that for a fixed magnetic field profile, e.g. $\beta = 0.1$ and $\gamma = 1$, the maximum mass decreases as \mathcal{B}_c increases from 10^{18} G to $4 \times 10^{18} \text{ G}$. Now as \mathcal{B}_c increases further from $4 \times 10^{18} \text{ G}$, with the same magnetic field profile (same β and γ), P starts decreasing with the increase of n_b at a very low n_b , leading to unstable matter. For $\mathcal{B}_c = 5 \times 10^{18} \text{ G}$, we obtain stable matter EoS for $\beta = 0.01$ and $\gamma = 2$, which deviates maximum from that without magnetic field, as shown in Fig. 8. It is found that the maximum deviation of mass-radius relation for $\mathcal{B}_c = 5 \times 10^{18} \text{ G}$ with respect to that without magnetic field is less than that deviation for $\mathcal{B}_c = 4 \times 10^{18} \text{ G}$ (see Fig. 7). Now if \mathcal{B}_c increases further to 10^{19} G , we note that (see

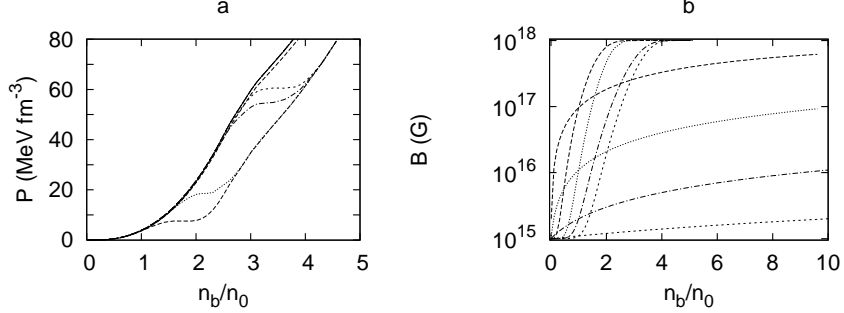


Figure 5: Variation of (a) P , and (b) B with normalized baryon number density for different magnetic field profiles with $\mathcal{B}_c = 10^{18}$ G. The solid curve is for without magnetic field. The sets of dashed, dotted, dot-dashed and short-dashed curves are for $\beta = 0.1, 0.01, 0.001$ and 0.0001 respectively. In each set (for each β), the upper curve in (a) is for $\gamma = 1$. The values of γ for the lower curve in sets in (a) are given in Table 2. In (b), for each β , the curves which reach \mathcal{B}_c at a comparatively lower n_b correspond to maximum γ cases.

β	γ	
	$\mathcal{B}_c = 10^{18}$ G	$\mathcal{B}_c = 3 \times 10^{18}$ G
0.1	4.0	1.4
0.01	6.0	2.6
0.001	6.0	3.5
0.0001	7.5	4.4

Table 2: γ -s for different lower curves shown in Figs. 5a and 6a for different β -s.

Fig. 9) with the above said profile ($\beta = 0.01$ and $\gamma = 2$) the matter becomes unstable at a very low density. We have stable matter up to a reasonably high density with $\mathcal{B}_c = 10^{19}$ G for $\beta = 0.001$ and $\gamma = 3$ with maximum deviation in EoS from that without magnetic field. However, Fig. 7 shows that in this case the deviation of EoS from that without magnetic field case is even lesser. Hence we can conclude that the effect of magnetic field is significant when \mathcal{B}_c is around 4×10^{18} G depending on the magnetic field profile. Beyond that, the magnetic field profiles needed to create significant effect of magnetic field on the mass-radius relation make the matter unstable.

As we have mentioned earlier, the effect of magnetic field on quark matter using the MIT bag model has been studied in many earlier work. Therefore,

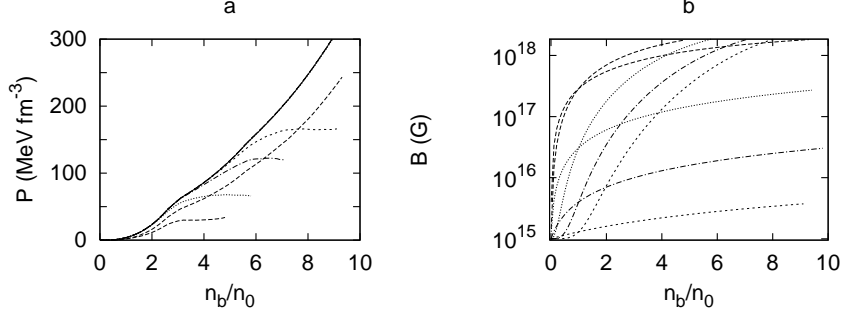


Figure 6: Same as Fig. 5 except for $\mathcal{B}_c = 3 \times 10^{18}$ G.

further it will be interesting to see the effect of magnetic field on other models, e.g. of Dey et al. [29], which is in progress.

4. Summary

We have studied the effect of high magnetic field on the NS matter. The nuclear matter inside the NS is highly dense (2 – 15 times normal matter density). We have considered the possibility of appearance of hyperons at the core of the NS with the increase of density. Our model is based on the relativistic mean field theory for nuclear matter. With the increase of density, the heavier particles appear gradually. However, due to repulsive potential, Σ -hyperons do not appear.

Observationally, the inferred surface magnetic field of a NS may be as high as 10^{15} G. It is believed that at the center, the magnetic field is higher than its surface value. As the density of matter also decreases with the increase of radius, we have taken the parametrization of the magnetic field as a function of density [49]. We have studied the effect of magnetic field on the NS matter with the different sets of parameters β and γ . We have found that the effect of magnetic field is important when $\mathcal{B}_c \geq 10^{17}$ G. On the other hand, when $\mathcal{B}_c \sim 10^{19}$ G, the matter becomes unstable. This gives a maximum bound of \mathcal{B}_c for NSs. For most of the X-ray and radio pulsars, the surface magnetic field ranges from 10^8 to 10^{12} G. It can be assumed that their central magnetic field is larger than their surface values by 3 – 4 orders of magnitude. Therefore, for this class of objects the effect of magnetic field is not significant. The effect of magnetic field can be observed only for magnetars whose surface magnetic field is $10^{14} - 10^{15}$ G and the central

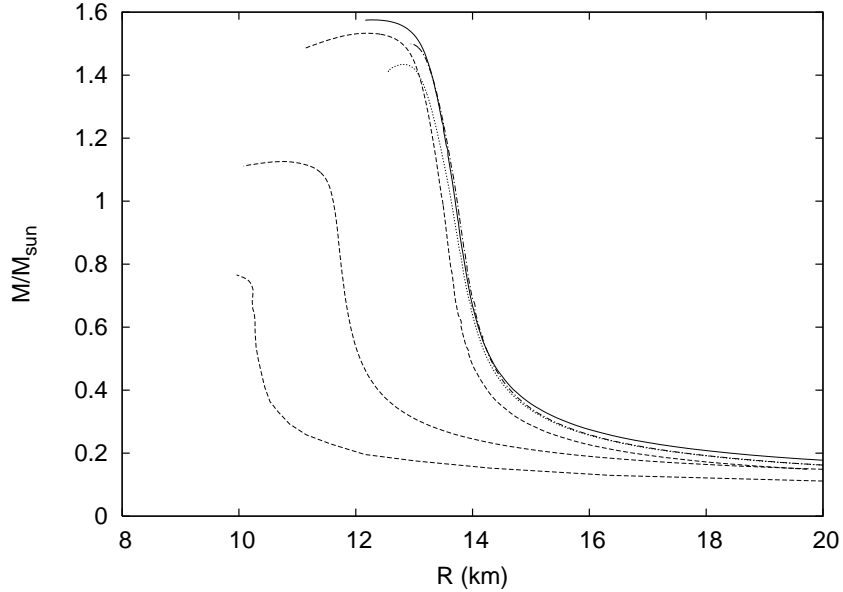


Figure 7: Mass-radius relations for static star with different values of \mathcal{B}_c . The solid curve is for without magnetic field. The dashed curves are for $\mathcal{B}_c = 10^{18}$, 3×10^{18} and 4×10^{18} G respectively from top to bottom for $\beta = 0.1$ and $\gamma = 1$. The dotted curve corresponds to $\mathcal{B}_c = 5 \times 10^{18}$ G for $\beta = 0.01$ and $\gamma = 2$, and the dot-dashed curve is for $\mathcal{B}_c = 10^{19}$ G when $\beta = 0.001$ and $\gamma = 3$.

magnetic field is constrained by the maximum value $\sim 10^{19}$ G. In reality also, we do not observe any compact object with ultra-strong magnetic field. This is consistent with the observed surface value of magnetars.

It should be noted that in strong magnetic field, there may arise anisotropic effect due to the magnetization of matter. However, in NS matter the magnetization is small [21]. In none of the previous work, this effect has been included. Therefore, it is expected that the inclusion of anisotropic effect might alter the present result quantitatively, but not qualitatively, leaving the conclusions unaltered. However, we have considered the field pressure contribution to the EoS of NS matter, which was not considered in any previous work.

In the presence of strong magnetic field, the nature of interaction between baryons may or may not be affected. However, the effect of magnetic field on nuclear interaction at very high density is poorly known till date, while nuclear interaction itself at high density is not well understood. Hence, we

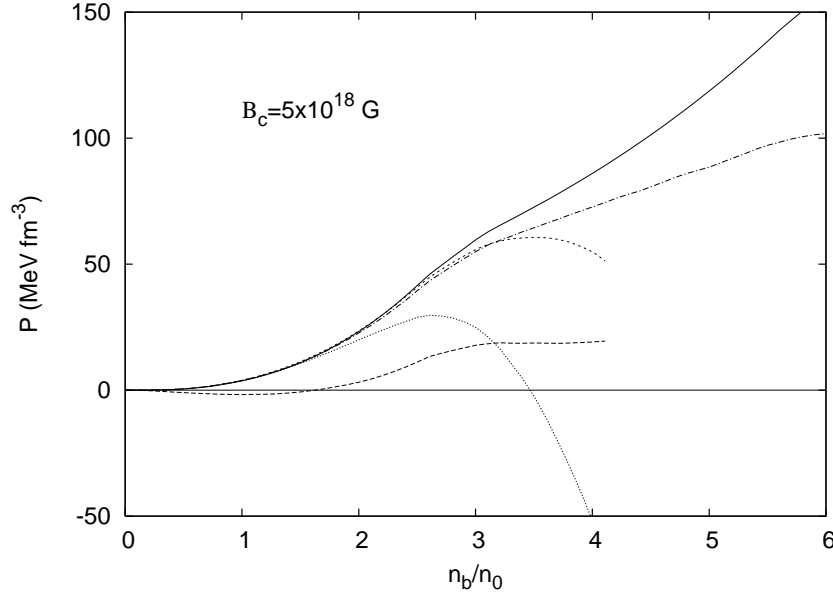


Figure 8: P as a function of normalized baryon number density with $\mathcal{B}_c = 5 \times 10^{18}$ G for different magnetic field profiles. The solid curve is for without magnetic field, the dashed curve for $\beta = 0.1$ and $\gamma = 1$, the dotted curve for $\beta = 0.01$ and $\gamma = 3$, the dot-dashed curve for $\beta = 0.01$ and $\gamma = 2$ and the short-dashed curve for $\beta = 0.001$ and $\gamma = 4$.

have employed the same model for baryonic interaction, what is widely used for nuclear matter without magnetic field. As our main aim is to study the properties of NS matter in presence of magnetic field, we do not study the magnetic field effect on the NS structure. It appears that the NS/magnetar structure with realistic EoS in presence of the magnetic field depends on the radial distribution of the magnetic field. Hence, a more realistic treatment including the effect on NS structure due to anisotropy arising from general relativity is expected to strengthen the present conclusions.

Acknowledgments

This work is partly supported by a project, Grant No. SR/S2HEP12/2007, funded by DST, India. The authors would like to thank Ritam Mallick of IISc for verifying one part of the computations.

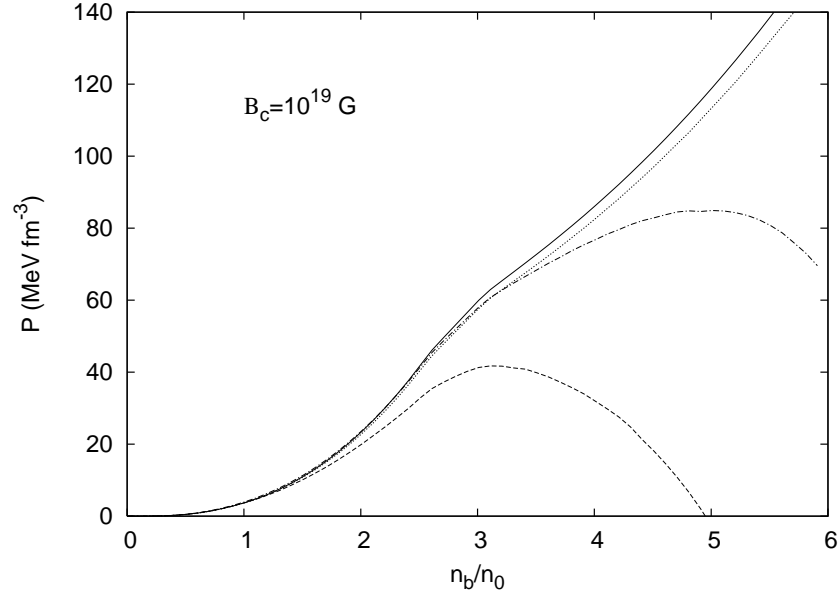


Figure 9: P as a function of normalized baryon number density with $\mathcal{B}_c = 10^{19}$ G for different magnetic field profiles. The solid curve is for without magnetic field. The dashed curve is for $\beta = 0.01$ and $\gamma = 2$, the dotted curve for $\beta = 0.01$ and $\gamma = 1$ and the dot-dashed curve for $\beta = 0.001$ and $\gamma = 3$.

References

- [1] A. Hewish, S. J. Bell, J. D. H. Pilkington, P. F. Scott, R. A. Collins, Nature 217 (1968) 709.
- [2] W. Baade, F. Zwicky, Phys. Rep. 45, (1934) 138.
- [3] F. Pacini, Nature 216 (1967) 567.
- [4] T. Gold, Nature 218 (1968) 731.
- [5] J. P. Ostriker, J. E. Gunn, Astrophys. J. 157 (1969) 1395.
- [6] D. C. Backer, S. R. Kulkarni, C. Heiles, M. M. Davis, W. M. Goss, Nature 300 (1982) 615.
- [7] M. A. Alpar, A. F. Cheng, M. A. Ruderman, J. Shaham, Nature 300 (1982) 728.

- [8] D. J. Morris et al., Mon. Not. Roy. Astron. Soc. 335 (2002) 275.
- [9] M. A. McLaughlin et al., Astrophys. J. 591 (2003) L135.
- [10] A. parmar, in *The Evolution of X-ray Binaries* Eds. Steve Holt and Charles S. Day. (New York: AIP Press) AIP conference Proceedings, Vol. 308, p. 415.
- [11] G. Vasisht, E. F. Gotthelf, Astrophys. J. 486 (1997) L129.
- [12] C. Kouveliotou et al., Nature 393 (1998) 235.
- [13] P. M. Woods et al., Astrophys. J. 519 (1999) L139.
- [14] R. C. Duncan, C. Thompson, Astrophys. J. 392 (19992) L9.
- [15] V. V. Usov, Nature 357 (1992) 472.
- [16] C. Thompson, R. C. Duncan, Mon. Not. Roy. Astron. Soc. 275 (1995) 255; Astrophys. J. 473 (1996) 322.
- [17] M. Bocquet, S. Bonazzola, E. Gourgoulhon, J. Novak, Astron. and Astrophys. 301 (1995) 757.
- [18] C. Y. Cardall, M. Prakash, J. M. Lattimer, Astrophys. J. 554 (2001) 322.
- [19] S. Chakrabarty, D. Bandyopadhyay, S. Pal, Phys. Rev. Lett. 78 (1997) 2898.
- [20] Y. F. Yuan, J. L. Zhang, Astrophys. J. 25 (1999) 950.
- [21] A. Broderick, M. Prakash, J. M. Lattimer, Astrophys. J. 37 (2000) 351.
- [22] W. Chen, P. Q. Zhang, L. G. Liu, Mod. Phys. Lett. A 22 (2005) 623.
- [23] F. X. Wei, G. J. Mao, C. M. Ko, L. S. kissinger, H. Stoecker, W. Greiner, J. Phys. G. 32 (2006) 47.
- [24] S. Chakrabarty, Phys. Rev. D. 54 (1996) 1306.
- [25] T. Ghosh, S. Chakrabarty, Int. J. Mod. Phys. D 10 (2001) 89; Phys. Rev. D 63 (2001) 043006.

- [26] R. G. Felipe, A. P. Martinez, H. P. Rojas, M. Orsaria, Phys. Rev. C 77 (2008) 015807.
- [27] R. G. Fowler, S. Raha, R. M. Weiner, Z Phys. C 9 (1981) 271.
- [28] S. Chakrabarty, Phys. Rev. D 43 (1991) 627.
- [29] M. Dey, I. Bombaci, J. Dey, S. Ray, B. Samanta, Phys. Lett. B 438 (1998) 123.
- [30] A. Li, R. X. Xu, J. F. Lu, Mon. Not. Roy. Astron. Soc. 402 (2010) 2715L.
- [31] A. E. Broderick, M. Prakash, J. M. Lattimer, Phys. Lett, B 531 (2002) 167.
- [32] J. D. Walecka, Ann. Phys. 83 (1974) 491.
- [33] S. A. Chin, Ann, Phys. 108 (1977) 301.
- [34] B. D. Serot, Phys. Lett. B 86 (1979) 146.
- [35] B. D. Serot, J. D. Walecka, Adv. Nucl. Phys., 16 (1986) 1.
- [36] J. Boguta, A. R. Bodmer, Nucl. Phys. A 292 (1977) 413.
- [37] N. K. Glendenning, Phys. Lett. B. 114 (1982) 392; Astrophys. J. 293 (1985) 470; Z. Phys. A. 326 (1987) 57; Z. Phys. A.327 (1987) 295.
- [38] F. Weber and W. M. Weigel, Nucl. Phys. A. 493 (1989) 549; 505 (1989) 779.
- [39] J. I. Kapusta, K. A. Olive, Phys. Rev. Lett. 64 (1990) 13; J. Ellis, J. I. Kapusta, K. A. Olive, Nucl. Phys. B. 348 (1991) 345.
- [40] Ellis J., Kapusta J. I., Olive K. A., 1991, NPB, 348, 345
- [41] K. Sumiyoshi, H. Toki, R. Brockmann, Phys. Lett. B. 276 (1992) 393; K. Sumiyoshi, H. Toki, Astro. Phys. J. 422 (1994) 700; K. Sumiyoshi, H. Kuwabara, H. Toki, Nucl. Phys. A. 581 (1995) 725; H. Shen, H. Toki, K. Oyamtsu K. Sumiyoshi, Nucl. Phys. A. 637 (1998) 435.
- [42] G. B. Cook, S. L. Shapiro, S. A. Teukolsky, Astrophys. J. 398 (1992) 203; 424 (1994) 823.

- [43] C. B. Dover, A. Gal, Prog. Part. Nucl. Phys. 12 (1984) 171.
- [44] J. Schaffner, C. B. Dover, A. Gal, C. Greiner, H. Stöcker, Ann. Phys. (N. Y.) 235 (1994) 35.
- [45] J. Schaffner and I. N. Mishustin, Phys. Rev. C 53 (1996) 1416.
- [46] T. Fukuda et al., Phys. Rev. C 58 (1998) 1306.
- [47] P. Khaustov et al., Phys. Rev. C 61 (2000) 054603.
- [48] S. Bart et al., Phys. Rev. Lett. 83 (1999) 5238.
- [49] D. Bandyopadhyay, S. Chakrabarty, S. Pal, Phys. Rev. Lett. 79 (1998) 2176.